JOURNAL OF MATERIALS SCIENCE 12 (1977) 2329–2342

Assessment of damage in GRP laminates by stress wave emission and dynamic mechanical measurements

G. D. SIMS, G. D. DEAN, B. E. READ, B. C. WESTERN*
Division of Materials Applications, National Physical Laboratory, Teddington, Middlesex, UK

Stress wave emission (SWE) and dynamic mechanical methods are described for monitoring the damage introduced into certain glass fibre-reinforced epoxy specimens by the application of a tensile load. For one particular composite system, a cross-ply laminate, it was possible to measure the concentration of damage by an independent optical method and correlations have been found between the SWE and dynamic mechanical results and the area of cracking. It remains to be established whether these correlations apply to other reinforcement geometries. This work is considered a first stage towards using these methods for monitoring the integrity of a component in service, from which its remaining life might be assessed.

1. Introduction

There is a need to develop non-destructive inspection techniques for composite materials suitable for the determination of component quality after fabrication, and for the assessment of degradation throughout service. This degradation often involves the formation of microcracks [1, 2] whose type, concentration and location depend on the reinforcement geometry and the type of loading. The formation of microcracks has been associated with the fall-off in residual strength and stiffness of fatigue loaded samples [3], but direct relationships and mechanisms have not been established. Microdamage can also be produced by creep [4], or thermal stresses [5], as well as by monotonically increasing stresses, and may degrade non-mechanical properties of design interest such as the impermeability and chemical resistance.

If techniques can be developed to assess the amount of damage in a component, then it may be possible to predict the remaining useful-life of the component during service. In addition, the assessment of component quality after fabrication may allow lower safety factors to be used in design through increased confidence that any component not meeting a minimum specification can be reliably detected. This increased confidence should result in a more efficient application of reinforced materials, particularly in situations involving critical design.

The methods which may be suitable for assessing the extent of damage in a specimen or component involve the measurement of dynamic mechanical properties and the monitoring of stress wave emission under stress. A number of papers [6–8] have reported recently that when certain composite systems are damaged by loading their dynamic stiffnesses are lowered whereas their damping factors increase. Liptai [9] has reported that the distribution of SWE counts with applied load obtained during tensile testing of aligned glass fibre-reinforced epoxy correlated well with a theoretical curve describing the statistical failure of glass fibres (assumed to be the source of emissions) in a bundle as a function of the applied load. In order to evaluate when these methods may be used reliably to predict integrity or remaining life, it is desirable to establish; (a) the type and concentration of damage introduced under different stress situations and reinforcement geometries, (b)

*Sandwich course student; now returned to Brunel University.

© 1977 Chapman and Hall Ltd. Printed in Great Britain.

how these influence the test measurements designed to monitor damage, and (c) how the damage reduces the useful life of the component. This paper is concerned with points (a) and (b) and reports the results of an initial programme in which specimens containing a range of different reinforcement geometries have been damaged by the application of a tensile load. The influence of the magnitude of this load upon the stress wave emission counts was determined and changes in the dynamic properties of the samples were measured. Dynamic stiffness and damping factor values were obtained both in flexure and in torsion. The results of the different detection methods have been compared and, where possible, related to measures of the damage determined by direct microscopic observation.

2. Damage detection techniques

2.1 Stress wave emission

Stress wave emission (SWE) techniques (alternatively referred to as acoustic or sonic emission) have been investigated for some time for the location of defects in large structures, such as pressure vessels [10]. It is only more recently that the technique has been applied to the analysis of failure mechanisms in materials, and in particular to composite materials [9, 11, 12].

The technique is based on the detection of the stress pulse generated by the strain energy released during deformation and fracture of the material. Only a proportion of the energy released by a fracture appears in the stress wave pulse. Before this pulse is detected by a transducer the pulse must propagate through the specimen from its source position to the transducer position, and through a couplant between the specimen and the transducer. The 'damage' will only be detected if it occurs during monitoring by SWE techniques, unless it can be inferred from the irreversibility of the emissions (known as the "Kaiser effect"). Consequently it is necessary to load the sample mechanically during monitoring if service loads or loads generated by other stresses, e.g. thermal, are not present. The necessity to apply an appreciable stress to the sample contrasts with most inspection techniques, but it may ensure that propagating cracks are detected in preference to physically larger but stable cracks. The load applied should preferably represent the loads expected to be experienced in service. It may be sufficient to determine the quality of the component to apply loads less than or equal to the service load rather than loads greater than the service load as used for proof test procedures. Continuous or intermittent monitoring may allow degradation during service to be followed.

The stress waves are normally detected by a piezo-electric transducer, and the resultant electrical signal can be processed in one of several ways (e.g. event counting, ring-down counting, count rate or total count). The value of more sophisticated signal analysis techniques has not yet been established, and there are additional difficulties in monitoring reinforced plastics due to signal attenuation (the use of SWE techniques and associated difficulties are discussed more fully elsewhere [13]). Consequently, a unit has been developed at NPL [14] which is a single channel system designed to determine the practical usefulness of simple, low-cost and portable equipment for failure analysis. This type of equipment may be suitable for quality control testing or in-service monitoring. This equipment was used in this study.

A piezo-electric transducer (AQ40-Environment Equipment Ltd) was clamped to the specimen by a constant load spring with a thin layer of high vacuum grease to provide good sonic contact. The electrical signal, which can be considered as a damped sinusoidal waveform, was amplified (80 dB) and low frequency extraneous noises filtered out. The resultant pulse was then recorded in the "ring-down" manner in which a count was recorded every time the pulse waveform crossed a pre-set voltage threshold. This method of counting gave an arbitrary weighting to the size of the pulse. The total number of counts was continuously displayed on a digital display and was available as a 0 to 10 V d.c. voltage that was simultaneously plotted with load against displacement using a multipen recorder.

2.2. Resonance methods

In the audiofrequency range (20 Hz to 20 kHz), dynamic moduli and associated damping factors are conveniently determined from resonance tests on materials in strip form. With this method, the specimen is successively driven into its various natural modes of vibration by a sinusoidal force of constant amplitude and variable frequency. When the driving frequency equals a natural vibrational frequency, a maximum is observed in the vibration amplitude. From the frequency of this so-called resonance peak, and the sample dimensions, the

real part of a complex dynamic modulus can be evaluated, and the damping factor is determined from the width (in Hz) of the resonance peak. Measurements on several resonance peaks, corresponding to different natural modes of vibration, enable the dynamic moduli and damping factors to be determined over a limited frequency range.

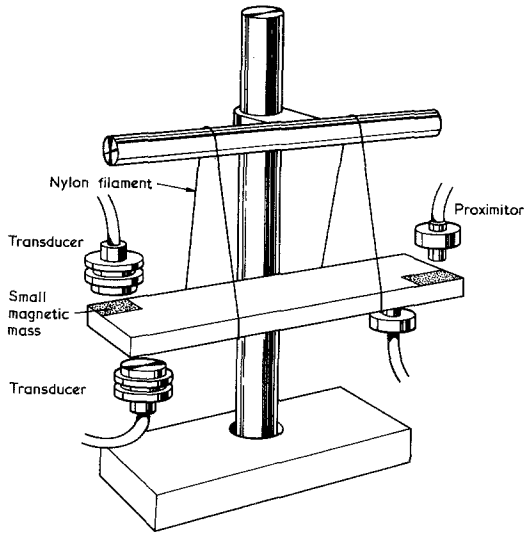

Figure 1 Resonance method.

The equipment employed at the NPL is designed to excite and detect either flexural or torsional modes of vibration, from which the dynamic tensile or shear moduli, respectively, and their associated damping factors can be obtained. As illustrated in Fig. 1, the bar specimen is suspended from two nylon filaments which are located at the nodal points for the particular vibrational mode under investigation. This type of suspension yields "free–free" modes of vibration and minimizes extraneous sources of added stiffness or damping. At one end of the sample two small magnetic steel masses are bonded at the corners, and sinusoidal forces are applied to them through two B and K electromagnetic transducers. The signals to the two transducers are derived from a common oscillator and individually amplified by separate power amplifiers. A balancing potentiometer enables the differential power to the two transducers to be continuously varied. By switching the phase of the signal to one transducer it is possible to apply either a net bending moment (out-of-phase currents), or a net twisting moment (in-phase currents). Vibration amplitudes are detected by two Bently Nevada proximitor probes each of which faces a small conducting mass (usually steel) bonded at the corners of the specimen opposite to the drive masses. The relative phase of the two detector signals is used to distinguish between flexural and torsional modes of vibration. Out-of-phase signals denote flexure and in-phase signals signify torsion. Resonance frequencies are read off directly from a frequency counter.

Flexural resonance modes have been principally employed in this study since the torsion pendulum (see below) was considered more convenient for studying certain effects such as non-linearity in the dynamic shear behaviour. From the flexural resonant frequencies f_n ($n = 1$, 2, 3 etc) effective dynamic tensile moduli E were calculated from,

$$E = 48\pi^2 \rho L^4 f_n^2 / h^2 K_n^2 \qquad (1)$$

where ρ, h and L are the sample density, thickness and length respectively and, for the free–free sample boundary conditions, the mode constant K_n has values of 22.373, 61.673 and 120.903 for $n = 1, 2$, and 3, respectively.

In the present work, values of E calculated on the basis of Equation 1 were corrected for effects due to the added drive and detector masses and for shear deformations and rotatory inertia. These correction procedures will be described elsewhere, and we note here only that the shear moduli required for shear corrections were derived from torsional resonance tests, and that the net corrections were small (<2%).

Flexural damping factors d_E were evaluated from the widths of resonance peaks. If Δf_n is the frequency difference between the two points on a peak having an amplitude $1/\sqrt{2}$ times the maximum amplitude then,

$$d_E = \frac{\Delta f_n}{f_n} \qquad (2)$$

The errors involved in the measurement of d_E were largest for the fundamental mode ($n = 1$) owing to the relatively sharp resonance peaks and high contributions from suspension losses and air damping. Consequently most of the data discussed in this paper relate to the 2nd flexural mode ($n = 2$) around 450 Hz. For this mode, errors in d_E arising from inaccuracies in the measurement of frequency were less than 5%, and contributions to d_E from suspension losses and air damping were estimated to be about 0.0008 for all samples.

It should be noted that the resonance method is an inherently low-amplitude test. For the 2nd flexural mode in these studies, root-mean-square tensile strain amplitudes between 0.5×10^{-6} and 8.4×10^{-6} have been calculated from the measured vibration amplitudes at resonance. The maximum tensile or compressive strain amplitudes on the specimen surfaces close to the antinodes are about 2.6 times these values. No dependence of the effective tensile moduli or damping factors on vibration amplitude could generally be detected within the amplitude range employed.

For a few specimens effective dynamic shear moduli and shear damping factors were measured from the fundamental torsional resonance peaks whose frequencies f_1 were in the range 1200 to 1700 Hz. Effective shear moduli were evaluated from,

$$G = \left(\frac{f_1 L}{h}\right)^2 \frac{(w^2 + h^2)}{[1 - 0.63(h/w)]} \quad (3)$$

where w is the specimen width. Small corrections to the G values were applied for the added inertia of the drive and detector masses. Shear damping factors d_G were calculated from an equation analogous to Equation 2 and air damping contributions to d_G were considered negligible. Although torsional resonance amplitudes were not monitored, average shear strain amplitudes were very low, of an order probably similar to the tensile strains deduced from the flexural resonance.

2.3. The torsion pendulum

The torsion pendulum is a well established instrument for measuring the dynamic shear properties of polymers. Compared with the torsional resonance method, measurements are made at lower frequencies, around 1 Hz, and at higher strains, 2×10^{-4} to 2×10^{-3}. The instrument used in this study employs an air-bearing to support an upper clamp, which is rigidly fixed to an inertia bar (Fig. 2). The specimen is held between the upper clamp and a fixed lower clamp so that when the inertia bar is displaced and released, the specimen performs damped torsional oscillations. The air-bearing contributes zero restoring torque and negligible damping and, therefore, does not influence the motion. The oscillations are detected by a rotary transducer mounted above the air bearing so that the period of the motion, P, and the amplitude of successive oscillations may be recorded electronically for the rapid and accurate acquisition of data. Measurements may be analysed by computer and the effective dynamic shear modulus G and damping factor d_G of the specimen are calculated using the equations:

$$G = \frac{4\pi^2 IL}{cwh^3 P^2} \quad (4)$$

$$d_G = \left(\frac{1}{\pi}\right) \ln \frac{A_n}{A_{n+1}} \quad (5)$$

where I is the moment of inertia of the torsion pendulum, A_n and A_{n+1} are successive oscillation amplitudes and c is a shape factor. G and d_G are only material parameters when the specimen is macroscopically homogeneous and isotropic in a plane normal to the axis of rotation.

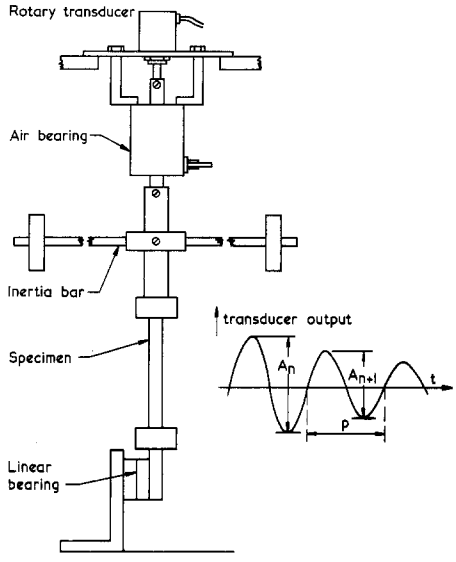

Figure 2 Torsion pendulum.

The inherent loss factor of the instrument is 1×10^{-2} and the deviation from the mean values recorded in the tables is usually less than 0.02×10^{-2}. The absolute accuracy in G is limited by non-uniformity in specimen thickness but changes in this property with damage for a single specimen can be detected very accurately being dependent only on the accuracy of period measurements. The data recorded in Table III relate to a maximum shear strain ϵ_{max} in the twisted specimen of approximately 1×10^{-3} obtained from the equation,

$$\epsilon_{max} = \frac{\theta_0 h}{L} \quad (6)$$

where θ_0 radians is the amplitude of the torsional oscillation at which measurements are recorded.

TABLE I Basic material properties of the laminates studied

Sample	Fibre direction	Density ($kg\,m^{-2}$)	Ultimate flexural strength ($MN\,m^{-2}$)	Dynamic properties of undamaged material	
				Flexural modulus ($GN\,m^{-2}$) (at ~ 1000 Hz)	Effective shear modulus ($GN\,m^{-2}$) (at ~ 1 Hz)
Cross-ply laminate* (Sheet A)	0°/90°	1977	221	19.5	5.2
Cross-ply laminate (Sheet A)	±45°	1977	123	14.9	8.2
Cross-ply laminate* (Sheet B)	0°/90°	2011	279	20.2	5.2
Chopped strand mat laminate	Random	1700	152	15.5	5.8
Woven fabric laminate	0°/90°	1683	146	16.7	3.0
Woven fabric laminate	±45°	1683	132	10.5	6.2

*The stress is directed as shown in Fig. 3.

3. Materials and experimental programme

Several geometries of glass fibre-reinforcement in epoxy resins have been studied. All the materials were obtained as press-moulded laminates from Permali (Gloucester) Ltd. The samples studied were a 0°/90° cross-ply laminate of aligned glass fibre/epoxy, a heavy weight glass fibre woven-fabric/epoxy and a chopped-strand glass fibre/epoxy. Samples of the cross-ply laminate and woven fabric laminate were tested at 45° to their principal fibre axes, as well as along these axes. The basic material properties for each of the materials, for the directions tested, are listed in Table I.

For the SWE and dynamic mechanical measurements, specimens 180 mm x 12 mm x ~ 1.7 mm were prepared with the required orientations from sheets of the laminates at least one metre square. The cross-ply material was used at the as-fabricated laminate thickness and the woven fabric and chopped-strand mat laminates were reduced from an original thickness of 6 to 7.5 mm. A fine-grade diamond saw was used for all preparations to minimize the possibility of introducing damage into the laminate at this stage.

The dynamic properties of each beam were determined as described in Sections 2.2 and 2.3. Subsequently the beams were gripped, with suitable protection, in hydraulically operated wedge-action grips on a 1251 Instron servo-hydraulic universal test machine. Only 10 mm of the specimen length was placed in each grip in order to minimize the volume of material not subjected to the full load, as the complete length of the beam formed the specimen in the flexural resonance technique. Specimens were loaded at a crosshead displacement rate of $1\,mm\,min^{-1}$ to pre-determined non-failing stress levels, while monitoring with the stress wave emission equipment, as described in Section 2.1. The dynamic properties of the beam were then re-determined. The edges of the cross-ply specimens were polished prior to testing so that the number and position of the cracks could be determined and the crack area per centimetre of sample length calculated (see Section 4.1). This was achieved using transmitted illumination, along the transverse fibre direction, and scanning the length of the specimen with an optical microscope fitted to a traversing facility.

Samples of the 0°/90° cross-ply laminate were studied further by incrementally loading two samples A and B, cut from sheets A and B respectively. Measurements were made of the dynamic properties and crack density after each increment of loading. The samples were loaded, using wedge action grips, in a Hounsfield Tensometer fitted with the stereo-microscope mentioned above thereby allowing observation of the cracks during loading. Stress wave emission was not used in these tests as there was the possibility of obtaining spurious counts each time the specimen was replaced and reloaded.

4. Results and discussion

4.1. Type and location of damage

The 0°/90° cross-ply laminates had the highest

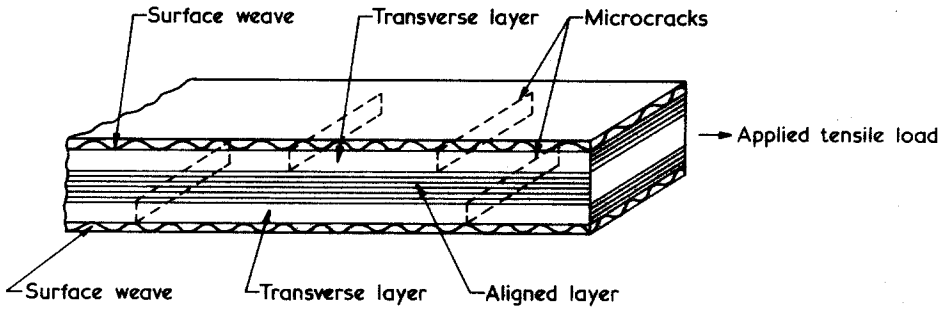

Figure 3 Showing the orientation of layers and micro-cracks in the 0°/90° laminate.

ultimate tensile strengths and can be considered to represent the class of angle-plied laminates favoured for critical applications such as in aircraft wing panels. The laminate used was constructed of five layers (Fig. 3); The centre three layers were of aligned glass fibres alternately orientated at 0° and 90°, with outside protective layers of satin weave fabric. The tests reported here were undertaken with the centre layer of fibres directed along the axis of the specimen. The other two layers of aligned fibres were transverse to the specimen axis and failed at low levels of applied strain by the formation of microcracks perpendicular to the applied stress which was directed along the specimen length. These cracks tended to propagate on formation across the whole width and depth of a transverse layer. Each microcrack was initially stabilized by the aligned layer and surface layers, and multiple fracture [15] of the two transverse layers by further transverse microcracking occurred as the load was increased. At higher loads, these microcracks propagated into the surface weave and along the interlaminar boundary, and final failure was controlled by longitudinal splitting and tensile failure of the centre-aligned layer. The microcracks occurred at or close to the interface of fibres perpendicular to the stress direction. This is the same failure mode that occurs in a unidirectionally reinforced composite material when a tensile stress is applied perpendicular to the fibre direction.

These same microfailures also occurred at low stress levels in woven fabric laminates and chopped-strand mat laminates. In these materials, the fibres transverse to the stress direction were in discrete bundles surrounded by pure matrix regions. Increased loading after the initial failures not only increased the number of microcracks but caused the microcracks to propagate into the resin-rich regions. The same failure mechanism was expected in materials tested at ±45° to the fibre axes. The effect of the initial microfailures on short and long term properties will depend on the direction and duration of all stresses present, and the presence of any aggressive environment such as water.

The tendency of the microcracks in cross-ply laminates to propagate fully across the cross-section of transverse layers allowed a direct measurement to be made of the total crack area in any specimen by surface observation of the number and position of the cracks. Observations were only made of the crack area for 0°/90° laminates because light transmission in ±45° material was insufficient to allow reliable detection of the cracks by optical microscopy. It was not possible to use surface observation of the other laminates to estimate the total crack area in the volume of the specimen as the initial damage is discontinuous.

Although sheets A and B are of the same construction there was a slight difference in the proportions of the central aligned layers. In sheet A, the transverse layers form 70% of the volume of the centre three aligned layers, compared to only 50% in sheet B (Fig. 4). Consequently the cracks in sheet A will have a proportionally greater effect on the dynamic properties and the ultimate strength of these samples will be similarly reduced.

4.2. Amplitude and frequency dependence of dynamic data

Prior to giving detailed consideration to the effects of damage on the results from each technique, it is appropriate to make a few comments about the amplitude and frequency dependence of the dynamic data. With the flexural and torsional resonance tests, no dependence of moduli or damping factors on strain amplitude could be detected for either undamaged or damaged specimens. This result is not too surprising in view of the very low strains involved (around 10^{-6}). In the case of the torsion pendulum, which operates over

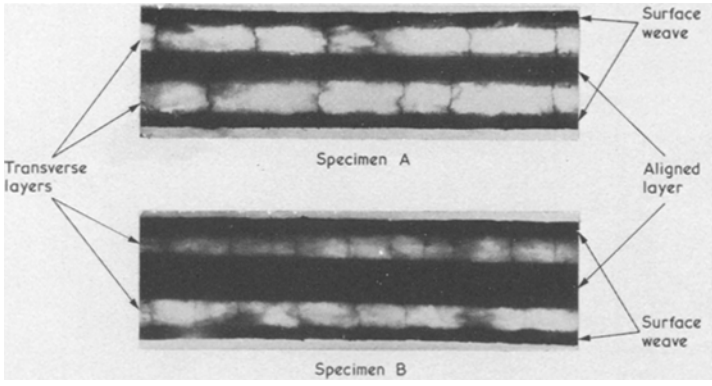

Figure 4 Relative proportions of each layer in specimen A and specimen B.

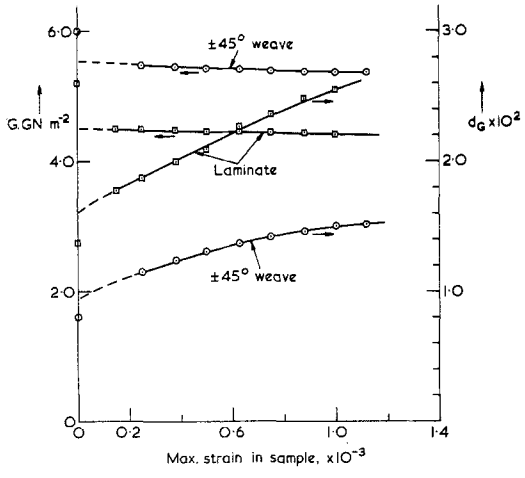

Figure 5 Dependence of effective shear moduli and damping factors of damaged 0°/90° laminate and ±45° weave samples upon test strain amplitude. Points on ordinate refer to data for undamaged samples.

a wider range of strains (2×10^{-4} to 2×10^{-3}) the observed moduli and damping factors were essentially independent of strain for the undamaged samples but they exhibited significant strain dependence for the damaged specimens. This result is illustrated in Fig. 5, where an appreciable increase in damping factor and a small decrease in shear modulus is observed with increasing strain amplitude for the damaged laminate and weave specimens. It will also be seen that the shear moduli for the undamaged samples are considerably higher than the moduli of the damaged samples extrapolated to zero strain, and that the damping factors for the undamaged specimens are significantly lower than the zero-strain damping factors for the damaged samples. However, the differences between the damping factors for undamaged and damaged samples at zero strain are small relative to the increase in damping factor with amplitude found for the damaged samples. Torsional reson-

TABLE II Frequency dependence of dynamic properties for undamaged specimens

Specimen	Flexure			Torsion		
	frequency (Hz)	E (GN m^{-2})	d_E	frequency (Hz)	G (GN m^{-2})	d_G
0°/90°	165.0	19.93	0.0097	1	5.20	0.0137
Laminate	457.6	20.19	0.0103			
	899.4	20.31	0.0112			
				1267	5.99	0.0230
Chopped-strand				1	5.10	0.0040
Mat	155.6	13.39	0.0039			
	446.2	14.48	0.0043			
	891.3	15.05	0.0047			
				1410	5.40	0.0065

TABLE III Comparison of data at high damaging loads for all materials studied

Sample	Applied load % Ult.*	SWE	E_D · GN/m²	$\frac{E_u}{E_D}$	$d_E^D \times 10^2$	$\Delta d_E \times 10^2$	$E_D \times \Delta d_E$ MN/m²	G_D · GN/m²	$\frac{G_u}{G_D}$	$d_G^D \times 10^2$	$\Delta d_G \times 10^2$	$G_D \times \Delta d_G$ MN/m²
0°/90° Cross-ply	66		17.3	1.17	1.24	0.21	36	4.57	1.14	2.2	0.83	38
laminate (Sheet A)	80		16.6	1.22	1.34	0.31	51	4.44	1.17	2.45	1.09	48
0°/90° Cross-ply	69	7 000	18.8	1.04	1.07	0.0	0	5.04	1.04	1.5	0	0
laminate (Sheet B)	88	130 000	16.0	1.22	1.14	0.075	12	4.64	1.13	1.9	0.4	19
± 45° Cross-ply laminate (Sheet A)	95	16 000	14.1	1.06	1.8	0.07	10	8.92	1.02	0.72	0.08	7
± 45° Cross-ply laminate (Sheet A)	92	23 000	12.2	1.10	1.9	0.25	30	8.04	1.02	0.78	0.13	10
Chopped-stand mat	75	200	16.1	1.00	0.47	0.04	6	5.8	1.0	0.40	0	0
Chopped-stand mat	95	7 000	14.1	1.03	0.50	0.08	12	5.0	1.02	0.49	0.08	4
0°/90° Woven fabric	70	700	15.8	1.05	1.1	0	0	2.76	1.07	2.5	0.69	19
0°/90° Woven fabric	90	6 500	15.8	1.06	1.05	0.05	8	2.72	1.12	2.7	0.90	24
±45° Woven fabric	63	7 000	8.81	1.20	2.5	0.34	30	5.64	1.10	1.2	0.32	18
±45° Woven fabric	77	61 000	7.56	1.40	2.6	0.45	34	5.28	1.15	1.7	0.80	42

*The scatter on the value for the ultimate tensile strength limits the reliability of these figures.

ance data on the 0°/90° laminate also revealed a shear modulus decrease with increasing damage at very low strains, but no significant change in damping factor could be found. In view of the marked amplitude dependence of the shear data obtained with the torsion pendulum, all results discussed below from this technique will refer to a fixed maximum strain amplitude of 10^{-3}.

The dynamic moduli and damping factors were generally found to increase with increasing frequency. This result is illustrated in Table II where comparisons are made between flexural resonance results derived from the lowest three resonant frequencies, and between shear data obtained with the torsion pendulum and torsional resonance method respectively. The results refer to undamaged laminate and chopped-strand mat material and are consistent with viscoelastic loss mechanisms in the epoxy matrix, since rigid epoxies are known to exhibit a damping maximum in the high audio–low ultrasonic frequency range. It should be added, however, that the frequency dependencies are small and observable only over a wide frequency range. Hence, the small changes in resonant frequency originating from the introduction of damage will have a negligible effect on the dynamic properties derived from a given technique.

4.3. Comparison of data for different reinforcement geometries

Table III summarizes the results obtained from the SWE, flexural resonance and torsion pendulum techniques for specimens of all materials investigated. For each sample the applied load is given as a percentage of specimen ultimate tensile strength. Changes in dynamic properties are recorded as a ratio of stiffness values and a difference between damping factors for the damaged and undamaged sample. Consideration of the accuracies of the dynamic test methods implies that relative changes in effective moduli of 1% and absolute changes in loss factor of about 0.04×10^{-2} define the limits of confidence of measurements made on the same sample. From Table III, comparisons can be readily made of the influence of damage upon dynamic properties for the different types of reinforcement and the angle which the stress axis makes with the major fibre directions.

For all the systems studied, dynamic moduli were found to decrease whilst loss factors increased with the introduction of damage. The decrease in modulus arises because, as cracks are introduced, material in the vicinity of the crack surface sustains less of the applied load. The load must be distributed to uncracked material resulting in higher extension for the same nominal cross-sectional area. If, during dynamic testing, frictional forces act at crack surfaces which are caused to slide, one relative to the other, then these will dissipate some of the energy of the vibration, enhancing the loss. Friction might, therefore, explain changes in the damping properties of the 0°/90° laminate and weave samples measured in torsion. The amplitude dependence observed in Fig. 5 indicates that these frictional forces are increasing as the relative displacement of the crack surfaces rises at higher strains.

Under flexure, the alternating tensile–compressive loading should serve to open and close cracks during vibration of the 0°/90° oriented samples and it is less clear how this might enhance damping. Local shear strains might be induced under tension in the matrix adjacent to the crack tip, and it is evident from data for the undamaged samples (Table II) that matrix shear deformations yield higher damping factors than do tensile deformations. Furthermore, in the flexural resonance test, shear stresses on cross-sectional planes are distributed along the length of the specimen and these exhibit maxima at the nodal points for the vibrational modes. For the lower modes of vibration, these shear stresses will not produce any significant shear strains for undamaged samples of high length/thickness ratio. However for damaged 0°/90° specimens they might induce sliding friction at the crack surfaces, and this effect could be enhanced in the laminates by the constraining effect of the outer layers of satin weave. In addition a contribution from sliding friction in the laminates might also arise if local delamination occurred at the boundary of the crack defined by adjacent layers. These frictional contributions may be expected to yield an increased damping factor with amplitude as observed in torsion but, as noted above, the strain range employed with the flexural resonance was too small to observe any significant amplitude dependence. If delamination is involved, then only an indirect correlation between changes in flexural properties and crack area might be expected (see below), and in the weave samples, there is less likelihood of delamination occurring. Hence it would appear that some mechanism associated with crack opening or sliding friction at

the crack surfaces induced by the shear stresses are the most likely explanations for the increased damping with damage observed in flexural resonance for the 0°/90° specimens.

The enhanced flexural damping observed in weave and laminate samples cut so that fibres are oriented at ±45° to the specimen length is presumably again caused by friction at crack surfaces since, under tension or compression, shear forces are established in the sample parallel to the crack faces which run parallel to the fibres. High stress wave counts for these samples might not necessarily imply a large crack concentration, since many counts could come from slipping at the crack faces as the tensile load is increased [16].

A quantitative approach to the interpretation of the dynamic data requires consideration of the energy dissipated in a cycle of the test per unit volume of material. For undamaged samples, this energy dissipation originates from viscoelastic loss processes and is proportional to $E_u d_E^u$ in flexure. Here E_u, the effective modulus of the undamaged sample, is proportional to the peak energy stored per cycle and d_E^u is the damping factor of the undamaged specimen. When cracks are introduced into the sample, the energy dissipated per cycle by viscoelastic loss processes may change owing to changes in the stress distribution under sinusoidal deformation. However, if we assume that the viscoelastic contribution to the energy dissipation changes in the same ratio as the peak stored energy, then this contribution becomes proportional to $E_D d_E^u$ where E_D is the modulus of the damaged specimen. Since the net energy dissipated per cycle in the damaged sample is proportional to $E_D d_E^D$, where d_E^D is the damping factor for the damaged material, it follows that the contribution to energy dissipation from the damage per cycle is proportional to $E_D(d_E^D - d_E^u) = E_D \Delta d_E$. This quantity is listed for each specimen in Table III together with the analogous quantity obtained from torsion pendulum data, namely $G_D(d_G^D - d_G^u) = G_D \Delta d_G$, where G_D is the effective shear modulus for the damaged sample and d_G^D and d_G^u are the damping factors for damaged and undamaged samples respectively. These quantities are considered most likely to correlate with crack density if the change in damping with damage stems directly from the cracks. A test of this correlation will be presented for the 0°/90° laminate below.

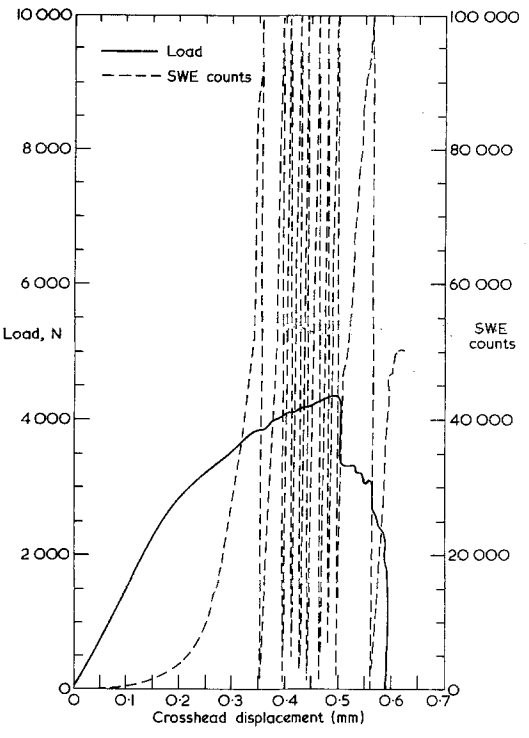

Figure 6 Failure of 0°/90° laminate sample showing variation of load and stress wave emission with applied displacement.

4.4. Correlation of test data with crack area for the 0°/90° laminates

We now consider in more detail results obtained on the 0°/90° laminates by the SWE, flexural resonance and torsion pendulum methods as a function of the measured crack areas. The load–extension curve for a 0°/90° laminate stressed along the single 0° layer is shown in Fig. 6. The deviation from linearity is at approximately 60% of the UTS and is due to the occurrence of microcracking. The SWE data predict damage prior to this deviation, an observation typical of glass-reinforced plastics and attributed to a small amount of microdamage, which is easily detected by SWE, but insufficient to produce a noticeable non-linear effect on the load-extension curve. The stress of this first emission may be useful in establishing a safe stress for long term strength and would provide a test method of assistance to design procedures in reinforced materials. Fig. 7 shows how the SWE counts vary with increasing amounts of damage, expressed as crack area per cm of sample length. These results are for six separate samples cut from sheet A, and detailed

crack observations showed that cracking occurred fairly uniformly along the specimen length as the applied load was increased.

Methods for interpreting SWE data, and in particular the correlation of the data with the micro-events taking place are still being developed using a range of materials and a range of tests. We have attempted to analyse the SWE counts in Fig. 7 by relating them to the strain energy released on crack formation.

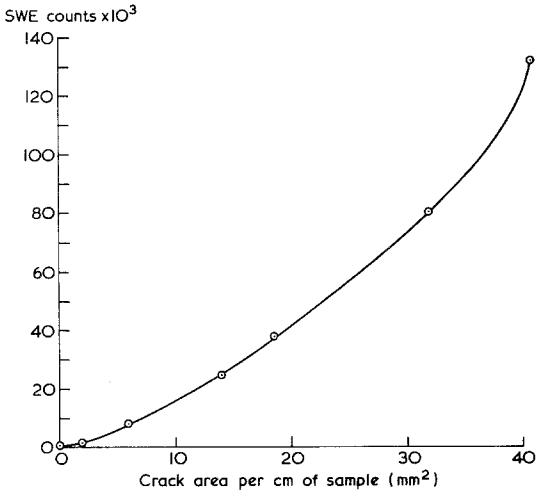

Figure 7 Increase in stress wave counts with crack area for 0°/90° laminate samples (sheet A).

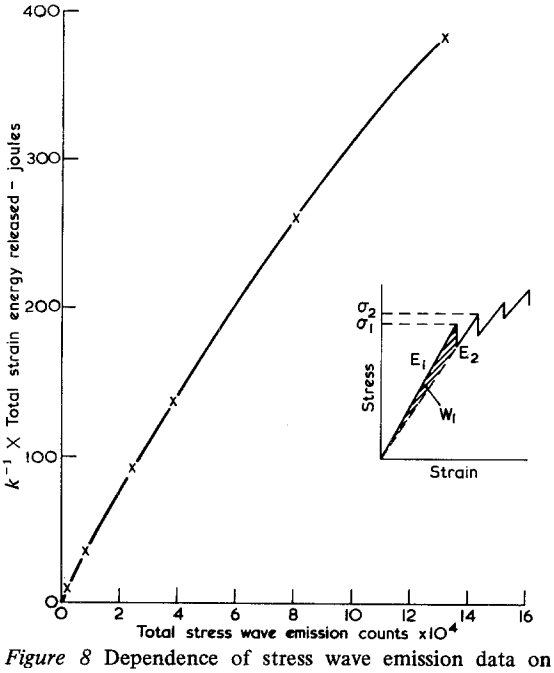

Figure 8 Dependence of stress wave emission data on strain energy released for 0°/90° laminate (sheet A).

Under fixed grip conditions the strain energy released (W_1) by the first crack per unit volume is given by

$$W_1 = \frac{\Delta\sigma_1 \cdot \sigma_1}{2E_1} \tag{7}$$

where σ_1 is the stress for the formation of the first crack, $\Delta\sigma_1$ is the fall in stress associated with the crack formation and E_1 is the initial modulus (Fig. 8, insert). The new (damaged) modulus of the specimen is E_2. This analysis considers a simplified specimen response where the unloading curve returns to the origin without any permanent set. Equation 7 can be rewritten as

$$W_1 = \frac{k_1\sigma_1^2}{2E_1} \tag{8}$$

where k_1 is defined as, $k_1 = \Delta\sigma_1/\sigma_1$.

It is now assumed that each subsequent crack occurs singly and at a uniformly increasing stress. Thus the second crack occurs at σ_2 and E_2 with constant k_2 where $\sigma_2 = \sigma_1 + \delta\sigma$ and $E_2 = E_1 - \delta E$. The incremental changes in stress and modulus, $\delta\sigma$ and δE respectively are obtained by dividing the total stress and modulus changes by the crack density for the specimen loaded to the highest stress. This is an acceptable approximation as both the applied stress and damaged modulus change in a linear manner over the range of crack observations. The strain energy released by the second crack is then given by,

$$W_2 = \frac{k_2\sigma_2^2}{2E_2}, \tag{9}$$

where

$$k_2 = \frac{\Delta\sigma_2}{\sigma_2}.$$

The total strain energy released by n cracks is then given by,

$$\sum_{x=1}^{n} W_x = \sum_{x=1}^{n} \frac{k_x\sigma_x^2}{2E_x} \tag{10}$$

or

$$\sum_{x=1}^{n} W_x = \frac{k}{2}\sum_{x=1}^{n} \frac{\sigma_x^2}{E_x}, \tag{11}$$

if k is assumed to be independent of the failure stress.

This strain energy term excluding the constant has been calculated for the 6 specimens in Fig. 7 using the dynamic modulus results for E_x and estimating σ_1 from a plot of crack density against

applied stress. In each case the energy term, multiplied by the specimen volume, has been normalized to eliminate the variation in crack area per crack between individual specimens. The relationship of this strain energy data to the stress wave emission data is shown in Fig. 8. The increasing deviation from a linear relationship could be due to the approximate nature of the theory used to obtain Equation 11 or to underestimating the crack area particularly at higher stress when secondary damage modes may be occurring.

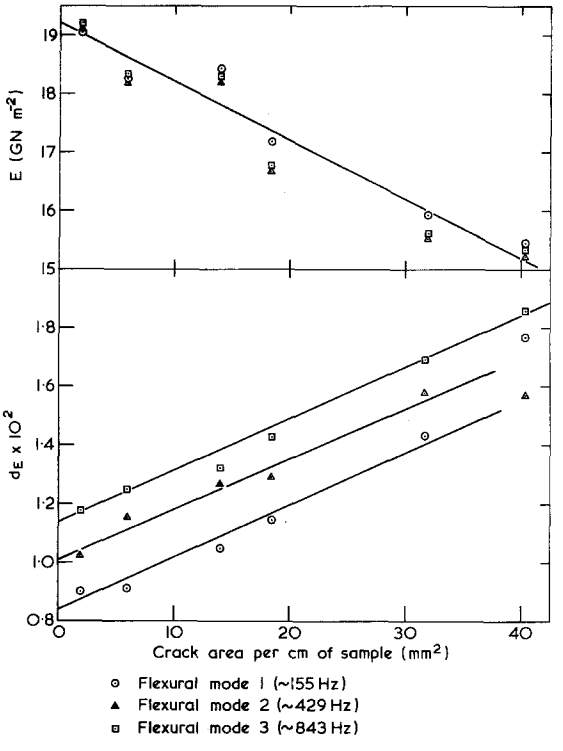

Figure 9 Dependence of effective flexural modulus and damping factor of 0°/90° laminate samples upon crack area (sheet A).

Although Equation 11 could be improved by calculating the value of k for each crack, this would still leave as unknowns the proportion of the strain energy released appearing as stress waves; the effect of specimen attenuation, particularly as the specimen is progressively cracked [17]; the effect of applied stress on specimen resonances which are known to effect stress waves [18]; and the effect of the scaling introduced by the use of ring-down counting. These limitations would also apply to more complex energetic solutions such as used elsewhere [15]. In addition, it may not be acceptable to use the dynamic moduli values to represent the change in moduli during loading. The present correlation has obvious limitations, but it does suggest that further research may enable an improved correlation between SWE data and the source micro-events to be obtained.

Fig. 9 illustrates the dependence of dynamic properties derived from the flexural resonance tests on crack area for those 0°/90° laminates which were also monitored by SWE (Figs. 7 and 8). Since the data were obtained for different samples cut from the same sheet, a considerable amount of scatter is observed but, despite this scatter, an approximately linear variation of both the effective modulus and flexural damping factor with crack area is seen for each of the three lower modes of vibration.

In order to minimize the uncertainty caused by experimental scatter, flexural resonance and torsion pendulum measurements were subsequently made on the two samples A and B which were each progressively loaded as described in Section 3, the dynamic measurements being effected between each increment of loading. As illustrated in Fig. 10, both the moduli and damping factors (plotted as ratios of the undamaged values) exhibit a linear increase with crack area, but the results for

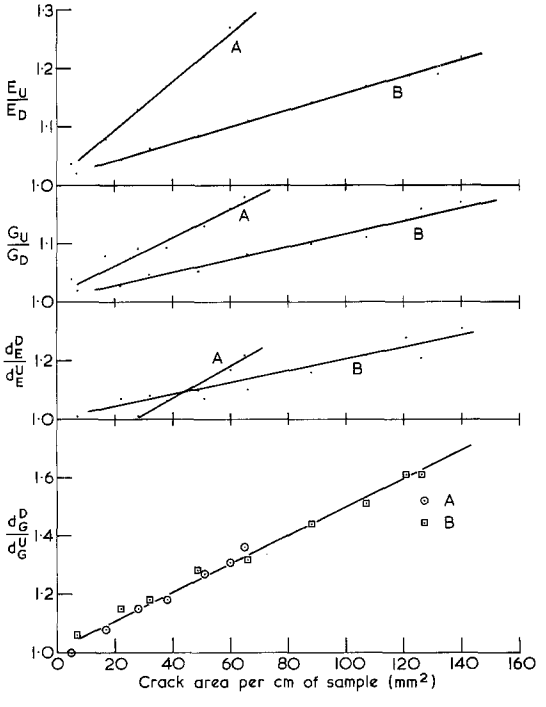

Figure 10 Dependence of moduli and damping factors measured in flexure and torsion upon crack area for single specimens cut from sheets A and B of the 0°/90° laminates.

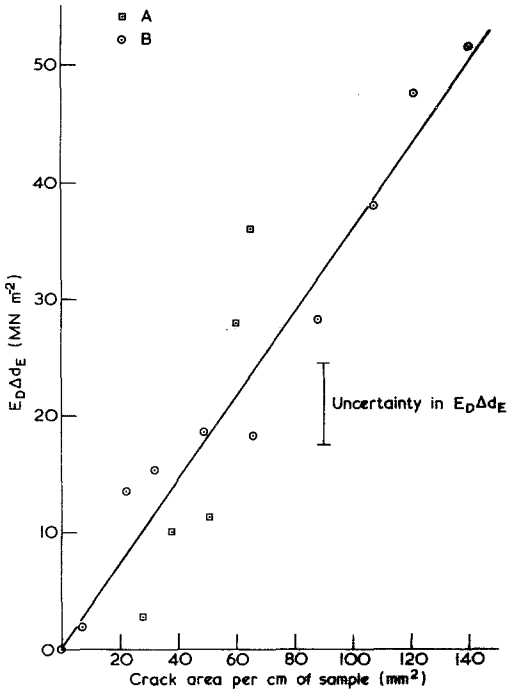

Figure 11 Dependence of $E_D\Delta d_E$ upon crack area for 0°/90° laminate samples.

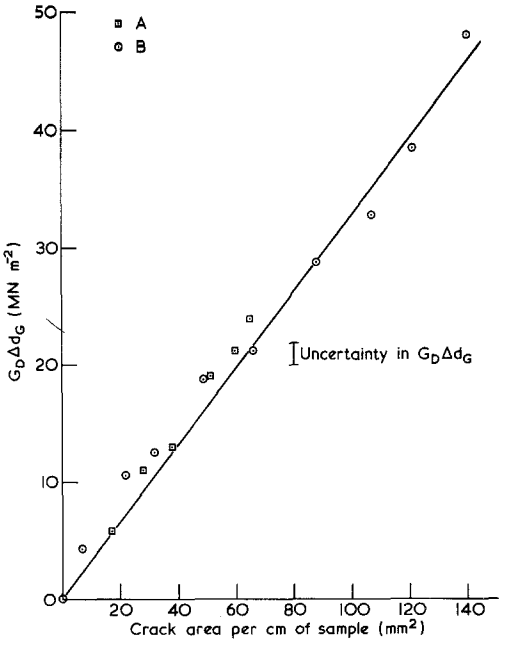

Figure 12 Dependence of $G_D\Delta d_G$ upon crack area for 0°/90° laminate samples.

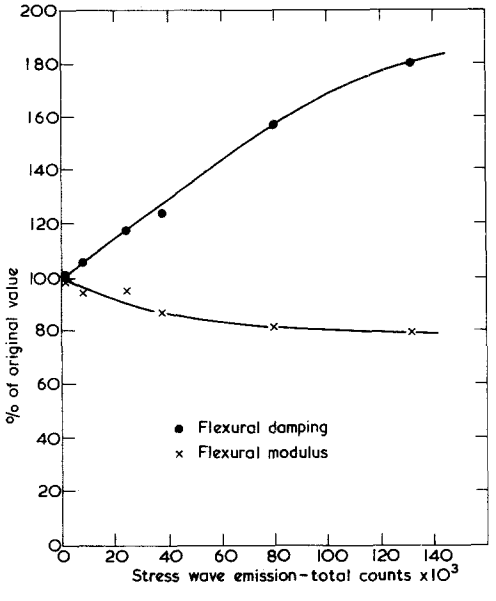

Figure 13 Comparison of stress wave emission data with percentage change in dynamic flexural modulus and damping.

the two samples A and B show appreciable differences. The observed differences are undoubtedly related to the variations in relative proportion of the different layers in each specimen, as discussed in Section 4.1.

In an attempt to eliminate variations in dynamic data due to slight differences in composition of specimens, and to obtain quantities relating to the contribution of the damage to the dynamic properties, plots have been constructed of $E_D\Delta d_E$ and $G_D\Delta d_G$ versus crack area. When plotted in this manner (Figs. 11 and 12) the dynamic data for samples A and B fall on the same straight lines within the estimated errors associated with the dynamic tests and indicated by the uncertainty limits. Slight deviations from the linear correlations in Figs. 11 and 12 might be expected owing to the non-uniformity of strain in the dynamic tests, which might render the positions of the cracks significant. Furthermore, for sample A small areas of delamination were observed under a microscope at the end of some cracks at high loads. This effect might explain the two high values of $E_D\Delta d_E$ for sample A in Fig. 11 at maximum crack area owing to the additional contribution to the energy dissipation. Nevertheless the linear correlations shown in Figs 11 and 12 suggest, according to the discussion in Section 4.3 that the principal influence of damage on the dynamic properties is to yield an additive contribution to the net energy dissipated per cycle which is proportional to crack area and which thus originates directly from the presence of cracks.

The test data obtained from dynamic methods and the SWE data for samples from Sheet A are directly compared in Fig. 13. Several thousand counts are recorded by the stress wave emission technique for a 5% change in dynamic properties. Although the stress wave emission technique has a higher sensitivity it is also susceptible to extraneous emission, and is limited in the majority of cases to detection while the specimen is under load. The dynamic methods do not suffer from these limitations and allow repeated measurement under different test (e.g. frequency, amplitude and mode) conditions.

5. Conclusions

Dynamic mechanical test methods and a stress wave emission technique have been used to monitor the presence of damage introduced into a range of glass fibre epoxy specimens by mechanical loading. For a $0°/90°$ cross-ply laminate, the number and area of cracks in a sample could be measured by optical microscopy and an important new correlation has been obtained between the crack area and the dynamic data. It has been shown that the total crack area in these samples is proportional to the energy dissipated per cycle by the cracks during dynamic mechanical testing. A good correlation was also obtained between the stress wave emission counts and the strain energy associated with crack formation calculated on the basis of a simplified model.

Whether dynamic mechanical measurements may be used to predict the concentration of cracks in samples containing other reinforcement geometries has yet to be established. This will require the determination of the concentration of cracks by an independent method. However, dynamic mechanical measurements are useful for the qualitative assessment of damage and complement the stress wave emission technique, in which higher sensitivities are obtained in the continuous monitoring of the introduction of damage in a specimen under a static or dynamic load.

The potential of these techniques for quantifying the occurrence of microdamage in reinforced plastics has been demonstrated. Before these methods might be used for assessing the quality of a component and its in-service performance, further work will be required to establish wider correlations between test data and damage. Also, the effect of damage on property degradation needs to be determined as well as how the results on laboratory specimens might be used to interpret data from components.

Alternatively, it might be valuable to evolve a direct correlation between dynamic and SWE measurements, and the remaining useful life of a component from measurements on the actual component under simulated service conditions.

References

1. L. J. BROUTMAN, *Modern Plastics* **42** (1965) 143.
2. M. J. OWEN, and R. DUKES, *J. Strain Anal.* **2** (1967) 272.
3. L. J. BROUTMAN, and S. SAHU, *ASTM S.T.P.* 497 (1972) 170.
4. A. D. S. DIGGWA, and R. H. NORMAN, *Plastics and Polymers* **40** (1972) 263.
5. M. J. OWEN, and S. MORRIS, *ibid* **40** (1972) 209.
6. A. B. SHULTZ, and D. N. WARWICK, *J. Composite Mater.* **5** (1971) 394.
7. A. T. DiBENEDETTO, J. V. GAUCHEL, R. L. THOMAS, and J. W. BARLOW, *J. Mater. Sci.* 7 (1972) 211.
8. R. D. ADAMS, J. E. FLITCROFT, N. L. HANCOX, and W. N. REYNOLDS, *J. Composite Mater.* 7 (1973) 68.
9. R. G. LIPTAI, *ASTM S.T.P.* **497** (1972) 285.
10. N. O. CROSS, L. L. LOUSHIN, and J. L. THOMPSON, *ASTM S.T.P.* **505** (1972) 270.
11. R. L. MEHAN, and J. V. MULLIN, *J. Composite Mater.* **5** (1971) 266.
12. E. G. HENNEKE, C. T. HERAKOVICH, G. L. JONES, and M. P. RENIERI, *Expt. Mechanics* **15** (1975) 10.
13. G. D. SIMS, NPL External Report IMS 29 (1975).
14. B. J. KEENE, and G. D. SIMS, *ibid* IMS 21 (1973) 21.
15. G. A. COOPER and J. M. SILLWOOD, *J. Mater. Sci.* 7 (1972) 325.
16. R. S. WILLIAMS, and K. L. REIFSNIDER, *J. Composite Mater.* 8 (1974) 340.
17. T. R. TAUCHERT, and N. N. HSU, *ibid* 7 (1973) 516.
18. J. M. SPEAKE, and G. J. CURTIS, Proceedings of International Conference on Carbon Fibres, their place in Modern Technology (Plastics Institute, London, 1974) Paper No. 29.

Received 31 December 1976 and accepted 4 April 1977.